

EFFECT OF SCREW DESIGN ON HOPPER DRAW DOWN BY A HORIZONTAL SCREW FEEDER

Justin W FERNANDEZ^{1*}, Paul W. CLEARY¹ and William McBRIDE²

¹CSIRO Mathematical and Information Sciences,
Private Bag 33, Clayton South, Victoria 3169, AUSTRALIA

²The University of Newcastle, Mechanical Engineering,
Callaghan, NSW 2308, AUSTRALIA

*Corresponding author, E-mail address: Justin.Fernandez@csiro.au

ABSTRACT

Screw feeders are used extensively in the food, plastics, household products, mineral processing and agricultural industries to remove material from hoppers and bins at a controlled rate. A key design requirement is to make the empty space in the screw available evenly along its exposed length below the hopper or bin. The evenness of the flow depends on the drawdown flow pattern, which in turn depends on the screw and hopper design, shape of the particles and wall friction effects. If the drawdown is not even then compositional variations in the outgoing stream can be created. The strongly varying residence time distributions for particles within the bin can also lead to quality issues. Designs to date have typically been based on analytical models and often performance issues are observed when the screw design used does not give the desired flow pattern. In this study the Discrete Element Method (DEM) is used to simulate particle transport in a horizontal screw feeder system for a range of conventional screw designs including variable screw pitch, screw flight and core diameters. The influence of screw design on the particle mass flow rate, the evenness of particle drawdown from the hopper and power consumption are investigated. The results of this study are able to better inform the design of screw feeders for specific materials. This has implications for product quality control, reduced power consumption and reduced wear on conveyer components.

NOMENCLATURE

x Distance along the screw (m)
 $Q(x)$ Mass flow rate along hopper trough (kg/s)
 η_V Volumetric efficiency
 $A(x)$ Cross-sectional area of the screw flight (m²)
 $p(x)$ Pitch of the screw flight (m)
 ω Angular screw velocity (rev/s)
 ρ Bulk density (kg/m³)

INTRODUCTION

Screw feeders are used to draw down bulk materials from a hopper bin and transport them over short to medium distances (typically up to 8 m) and generally provide good throughput control. The setup typically consists of a hopper bin, screw casing and a screw (Fig. 1). The screw rotates and draws down material from the hopper and transports it along the casing. While mechanically simple in principle, the behaviour of material during the draw

down process and transport can be complex (Cleary, 2007; Owen and Cleary, 2009). Unfortunately, most designs are based on analytical models that are limited by their continuum roots in terms of being able to predict the amount of material dragged in the screw boundary layer and in the internal shear and movement of the particles about the screw (Roberts et al., 1962 & 1993; Roberts, 2002). Previous DEM studies have focussed on horizontal and vertical conveyers and comparisons between modelling and empirical data (Shimzu and Cundall, 2001), long screw conveyers using a periodic slice model (Owen et al., 2003), hopper draw down using an inclined screw conveyer (Cleary, 2004) and the effect of particle shape (Cleary, 2007). This study investigates the effect on total mass flow rate, mass flow rate distribution from different regions of the hopper, draw down patterns and power consumption arising for six screw designs. The screws in this study cover a wide range of commonly found designs including variations in outer blade diameter, inner core taper and screw pitch spacing.

MODEL DESCRIPTION

Discrete element modelling

The Discrete Element Method (DEM) is the numerical tool used in this study and has been previously used to study the granular flow of material (Cleary 1998, 2002, 2004). DEM simulates granular flow by tracking individual particles and predicting their interactions between one another and external objects such as the screw and hopper. The particles can be modelled as spheres or blocky shaped particles. A contact law is used to derive contact forces from the instantaneous positions, orientations, velocities and spins of the particles. The present study uses a simple linear-spring dashpot model. The contact overlap scaled by a spring constant provides a repulsive force coupled with a dashpot to dissipate a proportion of the kinetic energy in a collision. In a similar way, the tangential force has an incremental spring based on the tangential displacement and a dashpot to dissipate tangential energy. For more details of DEM and the implementation used in this study see Cleary (1998, 2004) and Cleary and Sawley (2002).

Model setup

Six screw variants covering the range of different screw types encountered in industry are shown in figure 1 with geometric dimensions given in table 1. They include

changes in screw flight diameter (the outer diameter of the helical screw thread), screw core (the diameter of the central screw shaft), and pitch (distance from one thread peak to the next). The screws are:

- (i) constant flight diameter, constant core and constant pitch (screw A);
- (ii) tapered flight diameter, constant core and constant pitch (screw B);
- (iii) constant flight diameter, constant core and variable pitch (screw C);
- (iv) constant flight diameter, variable pitch and tapered core (screw D);
- (v) an expanding flight diameter, tapered core and constant pitch (screw E);
- (vi) 'optimised' parabolically expanding flight diameter with tapered core and a variable pitch (screw F).

The screw variants and the hopper bin and trough were modelled using CAD and the geometries were meshed using volume tetra elements at a resolution of 2 mm to capture the screw curvature.

The hopper bin was filled to approximately 80% full with 5 mm spherical grains resulting in ~100k particles and a mass of 8.8 kg. This were chosen to be comparable with commonly found grains including wheat and sorghum. Particles in the hopper bin were coloured in five evenly spaced vertical bands to allow quantification of draw down from different regions of the hopper (Fig. 2). For the analysis, particles initially inside the trough and surrounding the screw were ignored so that the predicted flow rates were based solely on draw down from the hopper bin. The mass flow rates were sampled at six evenly spaced locations along the screw length. After filling, the bulk density of the particles was ~733 kg/m³. The coefficient of restitution used was 0.5 and the coefficients of friction between particles, hopper wall and screw face were 0.6, 0.45 and 0.364, respectively. The contact spring constant was 1000 N/m producing an average contact overlap of ~0.5%.

The predicted mass flow rates were evaluated against an analytical relation (see the work of Roberts et al., 1962,1993; Roberts, 2002) for an angular screw velocity of 1 rev/s. Specifically, total mass flow rate, $Q(x)$, along the screw length, x , is given by

$$Q(x) = \eta_v(x) A(x) p(x) \omega \rho, \quad (1)$$

where $\eta_v(x)$ is the volumetric efficiency, $A(x)$ the cross-sectional area of the screw flight, $p(x)$ the pitch of the screw flight, ω the angular screw velocity and ρ the bulk density. The volumetric efficiency is the ratio of the actual flow to the maximum theoretical flow. The actual flow differs from the theoretical due to rotary motion and particle slippage between the screw and casing. The analytic solution used a wall friction angle of 20° on the screw surface. As this wall friction angle has been reported as an influential parameter (see the work of Roberts above), care was taken to include this in our simulations and assess its influence. For this study, the total mass flow rate along the hopper trough diameter, mass flow rate of each hopper colour region at the exit of the trough, and the power consumed over 30 seconds of real time was predicted using DEM.

HOPPER DRAW DOWN PATTERN

Figure 2 shows the draw down patterns in the centre plane of the hopper along the screw length. The rear and front walls of the hopper are on the left and right, respectively.

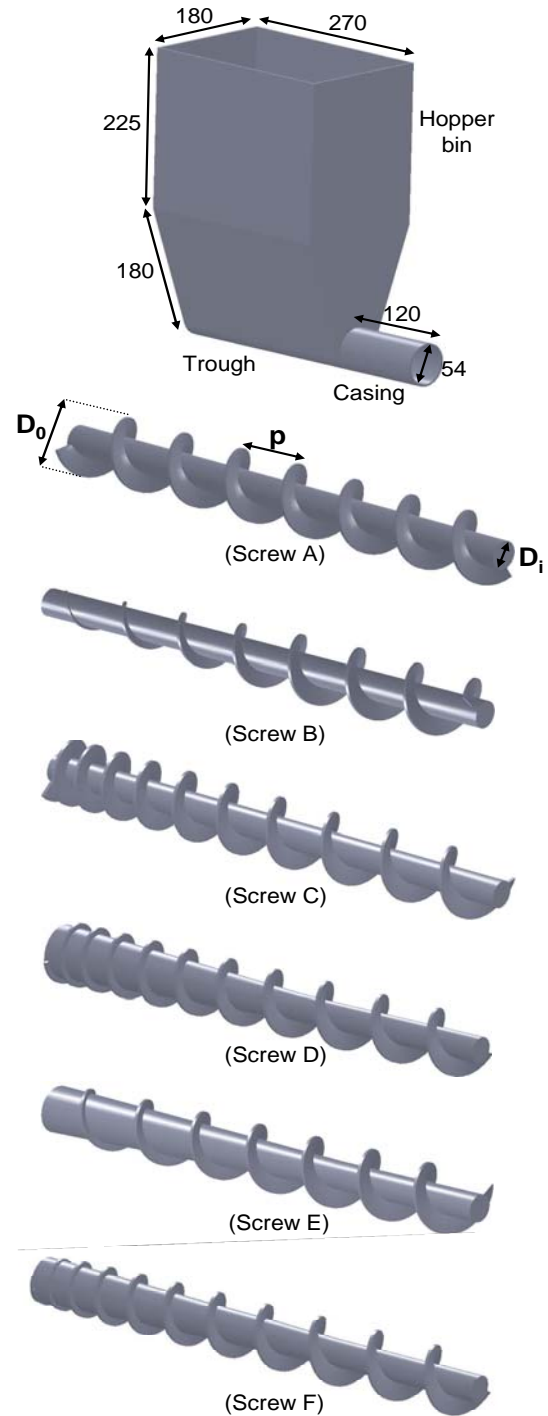


Figure 1: Hopper bin and screw casing geometry (mm); Screw A: standard, with labelled outer screw flight diameter (D_0), inner core diameter (D_i) and screw pitch spacing (p); Screw B: taper flight; Screw C: variable pitch; Screw D: variable pitch and taper; Screw E: tapered flight and core with constant pitch; Screw F: optimal flight, tapered core and variable pitch.

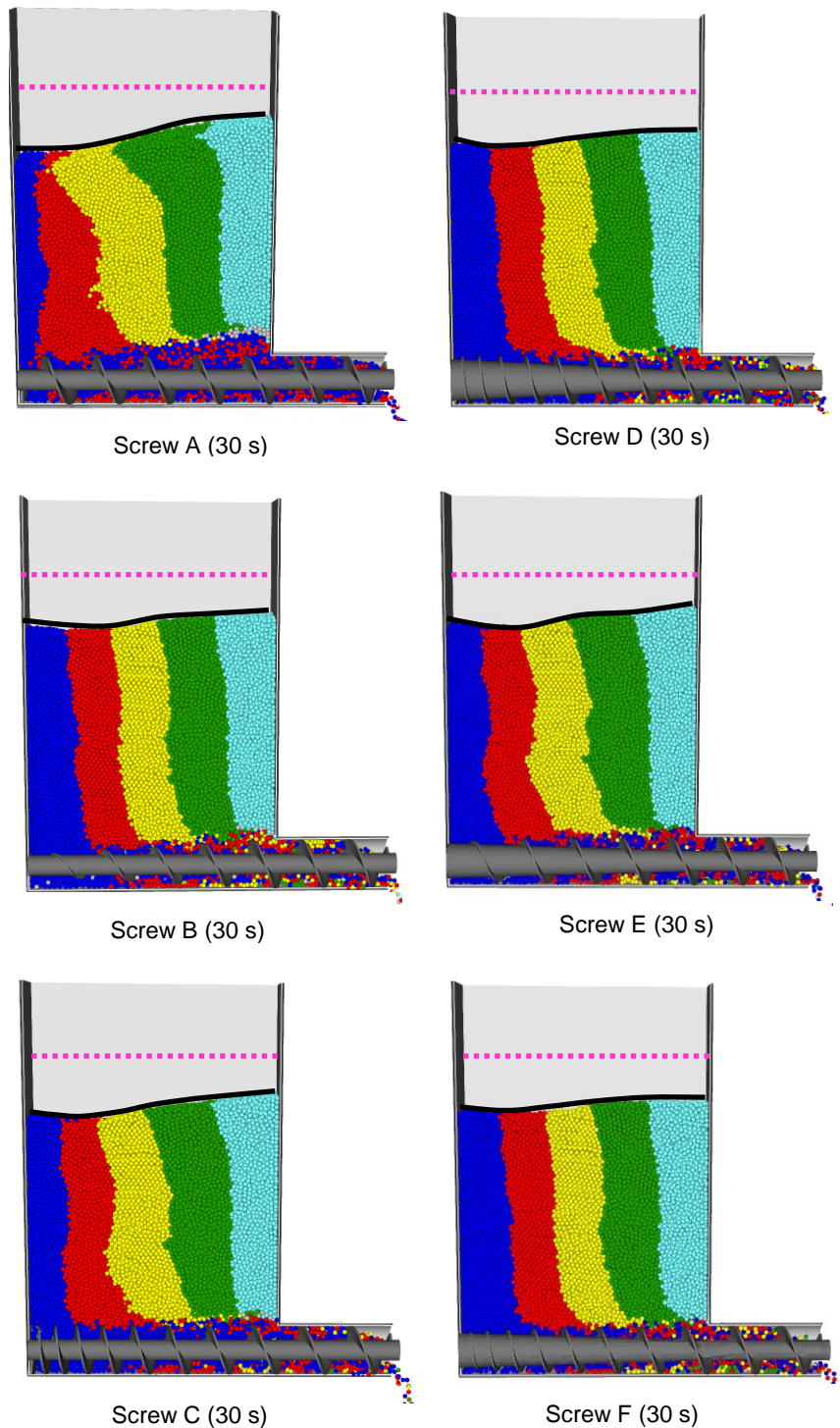


Figure 2: Hopper draw down patterns at 30 s in a central slice along screw length for screw A (standard), screw B (tapered flight), screw C (variable pitch), screw D (variable pitch and tapered core), screw E (tapered flight and core with constant pitch) and screw F (optimised flight, tapered core with variable pitch). The initial free surface is highlighted (pink dashed).

The standard screw (A) showed strong preferential draw down from the rear column (dark blue) of the hopper. Internal flow at the hopper rear was evident as the red material migrated towards the first two flights of the screw. Beyond the first two flights, no additional material could enter the screw volume, so no yellow, green or light blue particles reported to the discharged stream. The faster vertical settling of the rear columns gave rise to a free surface which dipped at the hopper rear. The effect on the

yellow and green columns was to flow towards the rear with the light blue column remaining roughly vertical. The yellow column also started to migrate internally towards the hopper rear. There was a significant quantity of entrained particles that could not fit through the hopper exit and were pushed up by the hopper front generating a recirculation pattern in the hopper. This has previously been reported (Cleary, 2007).

Screw B improved on the standard screw with an expanding flight that draws increasing amounts of material along the screw. This design delivered a fairly even vertical settling of all columns leading to a relatively flat free surface. All colours were detected at the hopper exit, however, in contrast to the standard screw, there was higher capture of the red column, followed by blue, yellow, green and light blue in decreasing order. In practice, screw B is often associated with stagnant material at the rear of the hopper due to reduced pull from the early small screw blades. Here we observed very slow migration of material from the rear trough rather than stagnation.

Screw C used an expanding pitch to progressively draw more material along the screw. The screw capture was biased towards the rear columns (dark blue and red) with lower capture by the middle and front columns (yellow, green and light blue). All colours except light blue were detected at the hopper exit. The fast vertical settling of the rear columns resulted in a slightly curved free surface that dipped at the rear, though not as pronounced as the standard screw (A). The red, yellow and green columns were slightly curved towards the hopper rear showing that particles in this region were drawn towards the rear screw flight. In contrast, the light blue column remained vertical.

Screw D combined both an expanding pitch and tapered core to further improve draw down over the standard screw. Screw D had the largest core diameter at the rear (45 mm). The reduced rear capture volume moved draw down capacity towards the front of the screw. All columns were drawn down fairly evenly, leading to a relatively flat free surface with all colours detected at the hopper exit. However, having two design features did not appear to provide significant improvement with the observed draw down being similar to screw B observed.

Screw E combined an expanding flight with tapered core to improve draw down capacity over the standard screw. Again, the extra features did not provide much difference from a simpler screw design like screw C (variable pitch). Specifically, screw E captured material preferentially from the rear columns (dark blue and red) with decreasing draw down of yellow and green. This produced a free surface that dipped towards the rear. There was no light blue material captured at the hopper exit.

Screw F combined three features; a tapered core, expanding pitch and tapered flight to improve draw down. This was most noticeable as all columns settled evenly along the free surface leading to the most level profile. This screw also created the least particle recirculation. All colours were detected at the hopper exit with screw F having the highest fraction of the light blue material. The amount of improvement in draw down was modest compared to screws B and D.

MASS FLOW RATES

The mass flow rates along the screw length are presented in two groups for clarity. Figure 3a shows constant core screws and figure 3b shows tapered core screws.

The DEM mass flow rate for screw A in figure 3a (blue-dashed) was nearly constant along the screw length after the first two flights. It shows clearly that almost all the material transported by the screw filled in the first 50 mm (first flight) and the last 10% over the second flight.

The analytic model (blue-solid) matched well, except at the hopper rear. This is due to the analytic model predicting a constant mass flow rate along the entire screw with all screw draw down at the extreme hopper rear. Figure 4 shows strong preferential rear draw for screw A with 80% dark blue material and 20% red material being present at the hopper exit.

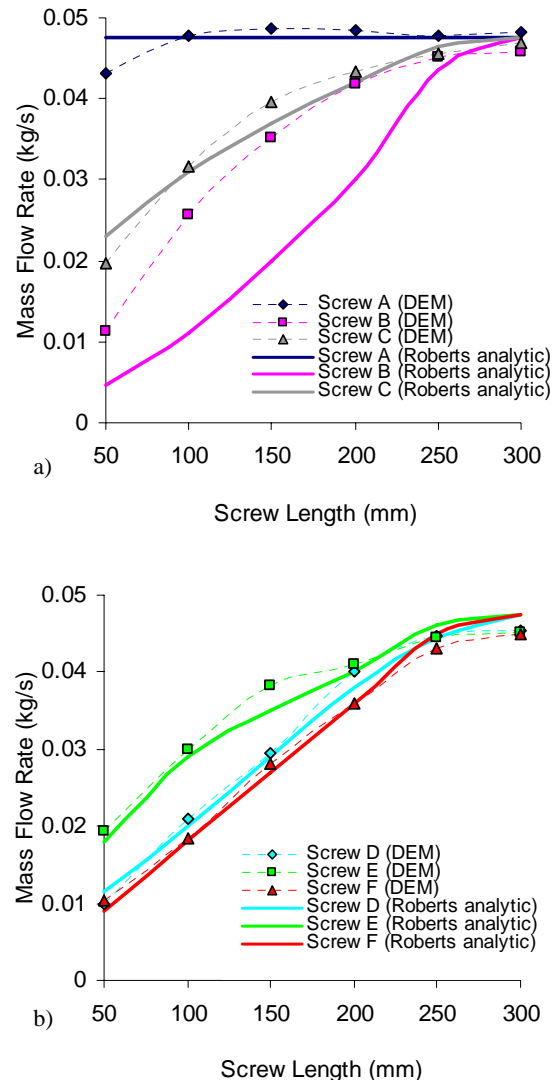


Figure 3: Comparison of predicted and analytic total mass flow rates along the screw from rear to front for screws with; a) constant core diameter, and b) tapered core.

The DEM mass flow rate of screw B (pink-dashed in figure 3a) was significantly lower than for the standard screw (A). This is consistent with the screw design, which was to draw less at the screw rear (due to a small blade diameter) and increase the draw down further along the screw by using an expanding tapered screw flight. About 25% of the screw transport volume filled in the first 50 mm. The second flight captured ~30% with the rate of draw down reducing after this point. DEM predicted a significantly larger mass flow rate than the analytic solution (pink solid) for screw B, especially towards the middle. This difference can be partially explained as eq. (1) computes the mass flow rate only using the cross-sectional area of the screw flight. For screw B, this is

considerably smaller being 22.5 mm at the rear. In contrast, the DEM simulation measured the actual mass flow rates which occur across the full hopper trough diameter (52.5 mm). Furthermore, in contrast to the DEM prediction, the analytic model for screw B showed an increasing mass flow rate gradient from rear to front. This suggests more material should be captured at the screw front than at the rear. However, DEM showed that this screw still gave preferential draw from the rear, which was different from the intended design. Figure 4 shows that screw B provides a colour breakdown (dark blue to light blue) of 37%, 29%, 22%, 10% and 1% of the total flow rate at the hopper exit. A much improved distribution over the standard screw but still far from even.

The DEM mass flow rate of screw C (grey-dashed in figure 3a) increased non-uniformly along the screw. Nearly 50% of the screw transport volume was captured in the first 50 mm (roughly two screw flights for this variable pitch). The draw down in the first flight was the second highest after the standard screw. Material capture by the screw decreased non-uniformly beyond this point. The agreement with the analytic model (grey-solid) was generally good. Figure 4 shows that screw C provides a colour breakdown (dark blue to light blue) of 54%, 32%, 12%, 2% and 0% of the total flow rate at the hopper exit. There is clearly a strong draw from the dark blue column with no light blue material captured by the hopper exit.

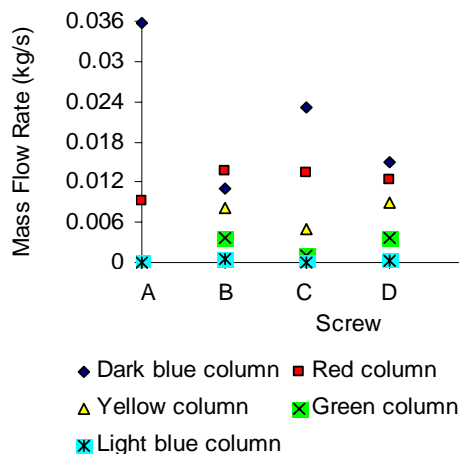


Figure 4: Mass flow rates of different coloured columns of particles in the hopper, measured at the exit of the hopper trough after 30 seconds.

The DEM mass flow rate of screw D (light blue-dashed in figure 3b) increased linearly for the first 250 mm of the screw length due to a combination of variable pitch and tapered core. About 20% of the screw transport volume filled in the first 50 mm (about two flights of the variable pitch). Beyond this the screw draw down was roughly constant until 250 mm. The agreement with the analytic model (light blue-solid) was good. Figure 4 shows that screw D provides a colour breakdown (dark blue to light blue) of 37%, 31%, 22%, 9% and 1% of the total flow rate. This shows that the first three columns dominated the particle makeup at the hopper discharge.

The DEM mass flow rate of screw E (green-dashed in figure 3b) increased non-uniformly along the screw due to a tapered core and flight. Nearly 40% of the screw fill volume was captured in the first 50 mm. The amount of material captured decreased along the screw length and

was negligible beyond 250 mm. The agreement with the analytic model (green-solid) was good. Figure 4 shows that screw E provides a colour breakdown (dark blue to light blue) of 52%, 33%, 12%, 3% and 0% of the total flow rate at the hopper exit. Similar to screw C, this design shows a strong preference for the rear column (dark blue) with no capture of the light blue material.

Screw F with variable pitch, tapered flight and core combined to give the most even capture along the screw. The DEM mass flow rate increased linearly over the first 250 mm of screw length (red-dashed in figure 3b). About 20% of the screw transport volume filled in the first 50 mm followed by constant capture till 250 mm. There was good agreement with the analytic model (red-solid). Figure 4 shows that screw F provides a colour breakdown (dark blue to light blue) of 31%, 32%, 22%, 12% and 3% of the total flow rate at the hopper exit. The first two colours were drawn fairly evenly with an improved proportion of green and light blue material. Despite giving the most even draw down it still demonstrates excessive draw down at the rear leading to still relatively low and restricted draw down at the front.

ENERGY AND POWER USAGE

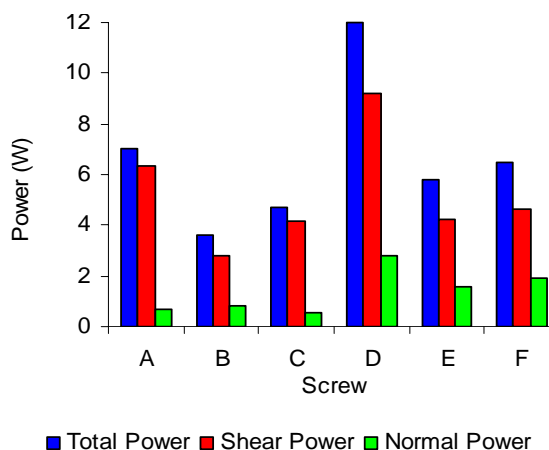


Figure 5: Total, shear and normal power usage.

Figure 5 shows that all screws used between 3.5 to 12 W of total power with shear being the main mechanism for energy dissipation (70% to 90% of total power). Shear power is associated with abrasive screw wear and particle degradation. The tapered core screws (D, E and F) also showed a higher normal power compared to the constant core screws. Normal power is associated with particle impact and breakage. Screw A, which had the poorest draw down had the second highest power draw. Of all the screw designs, screw B used the lowest total power and screw D the highest. A useful finding was that screws B, D and F, which had similar draw down patterns, produced substantially different power draws. Screw B used about half the power of screw F, which in turn used about half the power of screw D.

INFLUENCE OF FRICTION ON SCREW FACE

Figure 6 shows the influence of the screw face friction coefficient, which was investigated for the most optimal screw (F). Increasing the friction coefficient between the particles and the screw interface from 0.367 to 0.567 decreased the mass flow rate by a maximum of ~7%. This

friction increase was associated with roughly four times more power draw (6.5 W to 25.5 W). A friction reduction from 0.367 to 0.167 significantly increased the mass flow rate by up to ~30% with contributions from along the entire screw length. Power draw was only a quarter of the reference case (friction=0.367) after friction reduction (6.5 W to 1.6 W).

This demonstrates that screw feeder performance is quite sensitive to surface frictional properties and highlights the need for careful selection of flight material and finishing of the fabricated screw to ensure the designed functionality is achieved.

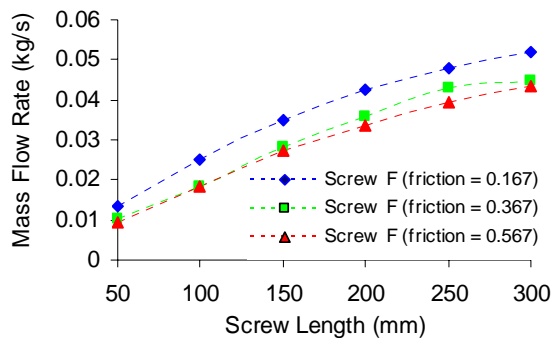


Figure 6: Effects of screw face friction on total mass flow rates for screw F.

CONCLUSION

Ranking the six screws based on the draw down of each colour and power usage placed screw F marginally first. It showed the most even draw down and colour particle capture at the hopper exit with an average power draw across all screws. Screw B was a close second in terms of draw down, but was observed to take longer to transport particles away from the hopper rear. In practice, this screw design is often associated with stagnant material in the rear due to a small blade diameter and can affect bulk material quality. Screw B provided the lowest power draw for a similar draw down to screw F. This would lead to lower wear and may provide operating cost savings. Screw D ranked third providing a similar draw down to screw F, but had twice the energy consumption. This screw could therefore have higher operating costs and shorter screw life. Ranked at fourth and fifth were screws C and E, respectively. They had similar preferential draw from the rear, but C used 20% less power than E. Screw A performed the poorest with no draw down from the front 60% of the hopper and had the second highest power draw. A general finding from this study was that screws with an expanding pitch and tapered core, or a simple tapered flight generate the most noticeable hopper draw down improvement over the standard screw.

Friction on the screw face was found to influence both power draw and mass flow rate. Specifically, a moderate increase in friction increased power draw by 10% while mildly reducing the flow rate. However, decreasing friction by the same amount significantly reduced power usage by 60% and increased mass flow by up to 30%. This emphasizes the importance of matching a bulk material with a suitably prepared screw surface.

The analytic method developed by Roberts et al. (1962 & 1993) matched the DEM results reasonably well. The one screw (B) where the results were significantly different highlighted a limitation of the analytic method.

Specifically, when a screw cross-sectional area is much smaller than the hopper trough that it resides in, the analytic method will under-estimate the flow which is based on screw cross-section only.

In summary, this study demonstrates the use of DEM to inform screw design through analysis of particle motion, region specific mass flow rates, power draw and frictional influence. DEM can assist with matching screw designs with specific bulk materials to enhance control of the draw down and to minimise power cost and wear.

REFERENCES

- CLEARY, P.W. (1998), "Discrete Element Modelling of Industrial Granular Flow Applications", *TASK. Quarterly - Scientific Bulletin*, **2**, 385-416.
- CLEARY, P.W. (2004), "Large scale industrial DEM modelling", *Engineering Computations*, **21**, 169-204.
- CLEARY, P.W. (2007), "DEM modelling of particulate flow in a screw feeder", *Progress in Computational Fluid Dynamics*, **7**(2-4), 128-138.
- CLEARY, P.W. and SAWLEY, M. (2002), "DEM modelling of industrial granular flows: 3D case studies and the effect of particle shape on hopper discharge", *Applied Mathematical Modelling*, **26**, 89-111.
- OWEN, P.J. and CLEARY, P.W. (2009), "Prediction of screw conveyor performance using the Discrete Element Method (DEM)", *Powder Technology*, **193**(3), 274-288.
- OWEN, P. J., CLEARY, P. W. and MCBRIDE, B., (2003), "Simulated granular flow in screw feeders using 3D Discrete Element Method (DEM)", *CHEMECA 2003*, ISBN 0-86396-829-5.
- ROBERTS, A. W., (2002), "Design and Performance Criteria for Screw Conveyors in Bulk Solids Operation", *Bulk Solids Handling*, **22**(6), 436-444.
- ROBERTS, A. W., MANJUNATH, K.S and MCBRIDE, W., (1993), "The Mechanics of Screw Feeder Performance for Bulk Solids Flow Control", *Trans. Mech. Eng., Institution of Engineers Australia*, Vol ME18 #1.
- ROBERTS, A. W., and WILLIS, A. H., (1962), "Performance of Grain Augers", *Proc. The Institution of Mechanical Engineers*, London, **197**(8), 67-73.
- SHIMIZU, Y., and CUNDALL, P. A., (2001), "Three-dimensional DEM simulation of bulk handling screw conveyors", *J. Engineering Mechanics*, **127**, 864-872.

APPENDIX

Screw	Outer blade Diameter (D_o) (mm)	Core shaft diameter (D_i) (mm)	Pitch (p) (mm)
A	52.5	22.5	52.5
B	22.5 - 52.5	22.5	52.5
C	52.5	22.5	12 - 52.5
D	52.5	45 - 22.5	12 - 52.5
E	37.5 - 52.5	37.5 - 22.5	52.5
F	37.5 - 52.5	37.5 - 22.5	12 - 52.5

Table 1: Geometric properties of the six screw designs.